Journal of Maps, 2016
Vol. 12, No. 1, 123–136, http://dx.doi.org/10.1080/17445647.2014.992177

Routledge
Taylor & Francis Group

SCIENCE

Glacial geomorphology of the Altai and Western Sayan Mountains, Central Asia

Robin Blomdin[a,b*], Jakob Heyman[b], Arjen P. Stroeven[b], Clas Hättestrand[b], Jonathan M. Harbor[a,b], Natacha Gribenski[b], Krister N. Jansson[b], Dmitry A. Petrakov[c], Mikhail N. Ivanov[c], Orkhonselenge Alexander[d], Alexei N. Rudoy[e] and Michael Walther[f]

[a]*Department of Earth, Atmospheric, and Planetary Sciences, Purdue University, West Lafayette, USA;* [b]*Bolin Centre for Climate Research, Department of Physical Geography and Quaternary Geology, Stockholm University, Stockholm, Sweden;* [c]*Faculty of Geography, Lomonosov Moscow State University, Moscow, Russia;* [d]*Department of Geography, School of Arts and Sciences, National University of Mongolia, Ulaanbaatar, Mongolia;* [e]*Department of Geology and Geography, Tomsk State University, Tomsk, Russia;* [f]*Mongolian Academy of Sciences, Geographical Institute, Ulaanbaatar, Mongolia*

(*Received 21 June 2014; resubmitted 5 November 2014; accepted 21 November 2014*)

In this article, we present a map of the glacial geomorphology of the Altai and Western Sayan Mountains, covering an area of almost 600,000 km^2. Although numerous studies provide evidence for restricted Pleistocene glaciations in this area, others have hypothesized the past existence of an extensive ice sheet. To provide a framework for accurate glacial reconstructions of the Altai and Western Sayan Mountains, we present a map at a scale of 1:1,000,000 based on a mapping from 30 m resolution ASTER DEM and 15 m/30 m resolution Landsat ETM+ satellite imagery. Four landform classes have been mapped: marginal moraines, glacial lineations, hummocky terrain, and glacial valleys. Our mapping reveals an abundance of glacial erosional and depositional landforms. The distribution of these glacial landforms indicates that the Altai and Western Sayan Mountains have experienced predominantly alpine-style glaciations, with some small ice caps centred on the higher mountain peaks. Large marginal moraine complexes mark glacial advances in intermontane basins. By tracing the outer limits of present-day glaciers, glacial valleys, and moraines, we estimate that the past glacier coverage have totalled to 65,000 km^2 (10.9% of the mapped area), whereas present-day glacier coverage totals only 1300 km^2 (0.2% of the mapped area). This demonstrates the usefulness of remote sensing techniques for mapping the glacial geomorphology in remote mountain areas and for quantifying the past glacier dimensions. The glacial geomorphological map presented here will be used for further detailed reconstructions of the paleoglaciology and paleoclimate of the region.

Keywords: glacial geomorphology; paleoglaciology; Altai Mountains; Western Sayan Mountains; remote sensing

1. Introduction

The Altai Mountains in Central Asia (Figure 1) consist of a series of NW-SE trending ranges with elevations up to 4500 m above sea level (a.s.l.), alternating with intermontane basins

*Corresponding author. Email: rblomdin@purdue.edu; robin.blomdin@natgeo.su.se

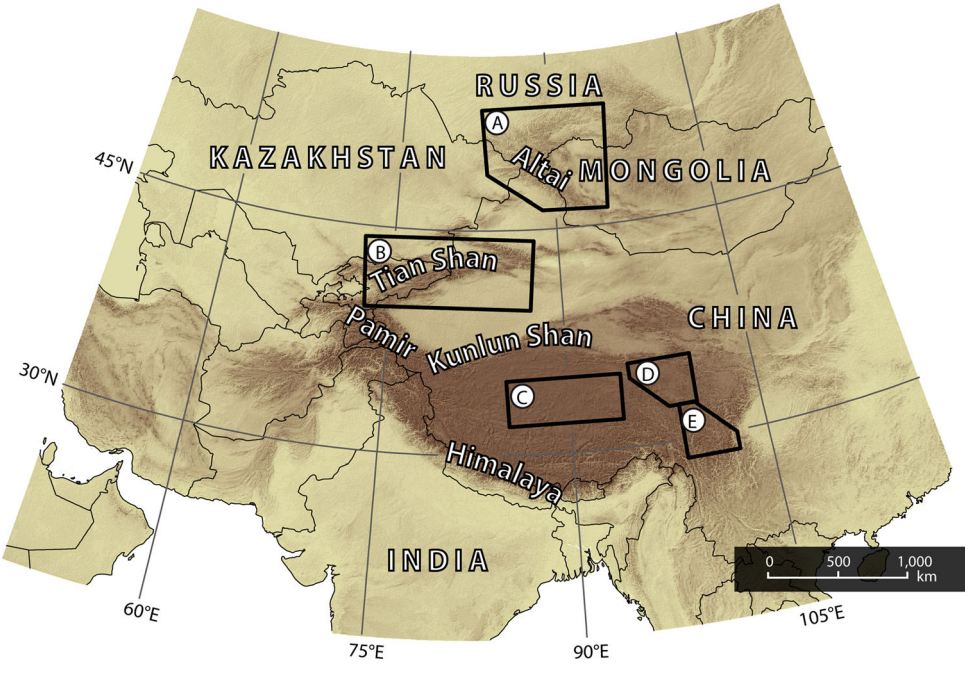

Figure 1. Location of the mapped area and previously published glacial geomorphological maps from Central Asia and the Tibetan Plateau. (A) Altai and Western Sayan Mountains (Fig. 2; this study). (B) Tian Shan (Stroeven et al., 2013), (C) Tangula Shan (Morén et al., 2011), (D) Bayan Har Shan (Heyman et al., 2008), and (E) Shaluli Shan (Fu et al., 2012).

(Tronov, 1949). These ranges straddle the borders between Kazakhstan, Russia, China, and Mongolia, connect with the Western Sayan Mountains to the north, and include isolated massifs extending eastwards into Mongolia (Figure 2). As with other Central Asian mountain ranges such as the Tian Shan, Pamir, and Kunlun Shan, the Altai Mountains act as a barrier for moisture travelling from the west and northwest leading to pronounced spatial variations in precipitation. Equilibrium line altitudes (ELAs) are therefore located around 3000 m a.s.l. in the more humid northwestern ranges of the Altai, while in the semi-arid and arid southeastern ranges the ELA is located around 3700 m a.s.l. (Lehmkuhl, Klinge, & Stauch, 2004). The limited extent of glaciers in the eastern Russian Altai and Mongolian Altai is the result of decreasing precipitation and increasing ELAs from west to east (Dolgushin & Osipova, 1989; Lehmkuhl et al., 2004; Tronov, 1949). Present-day glaciers occupy the highest mountains of the Altai but the estimates of glacierized area remains uncertain. For example, Shi (1992) estimated the total glaciated area in the Chinese Altai as 300 km^2, Bussemer (2000) estimated the area of glaciers in the Russian Altai as 900 km^2, and Klinge (2001) estimated the contemporary glacier coverage in the Mongolian Altai as around 850 km^2. To our knowledge, only Okishev (2006) present estimates of the total glaciated area (1562 km^2) for the whole Altai. Recent studies of contemporary glaciation in the Altai Mountains have focused upon individual mountain ranges and massifs (e.g. Kamp, McManigal, Dashtseren, & Walther, 2013). For example, Kamp et al. (2013) estimated the total glacier coverage of the Ikh-Turgen massif (Figure 2) as 31.8 km^2. Valley glaciers in the Altai region are the sensitive indicators of both regional and local climate (Tronov, 1966), and on the time scale of a glacial cycle they respond to variations in the strength and position of different climate systems. Meltwater from the glaciers in the Altai also feed several large rivers, including the Katun and Biya, which are sources for the Ob river (Figure 2).

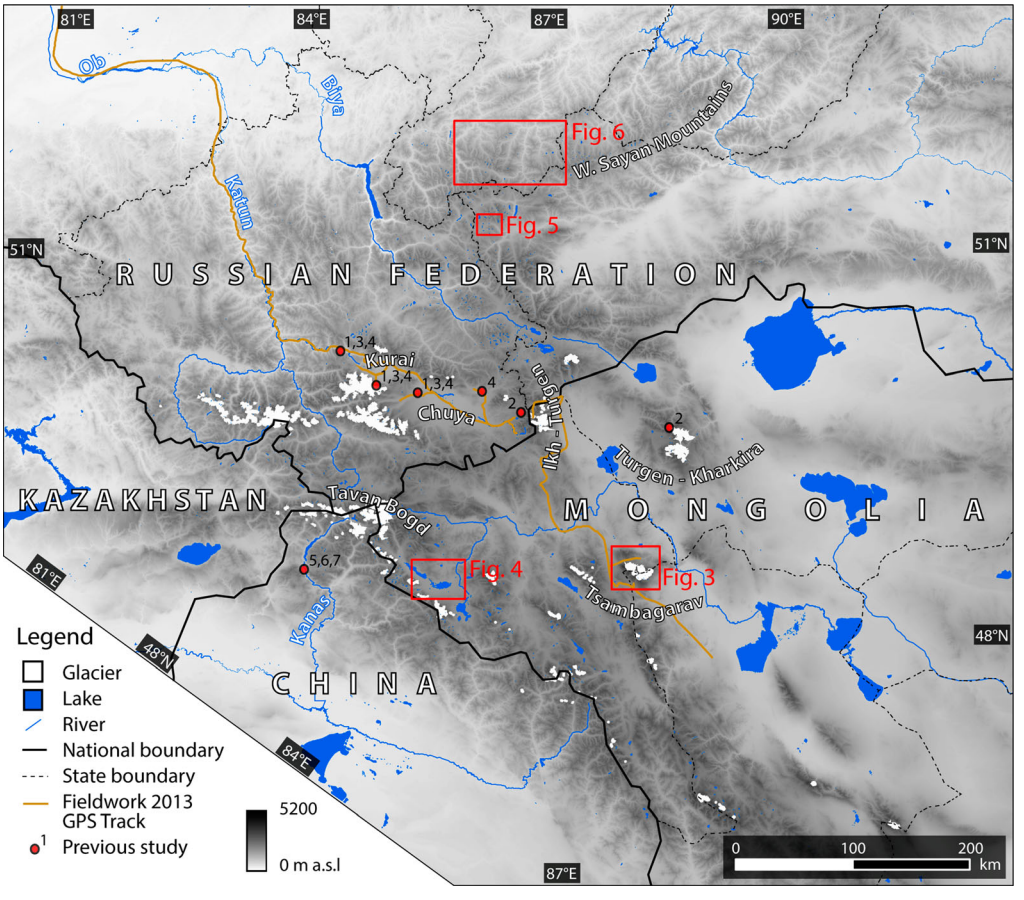

Figure 2. Physiography and administrative borders of the Altai region. The locations of previous studies of paleoglaciology and glacial geomorphology are shown: (1) Rudoy (2002), (2) Lehmkuhl et al. (2004), (3) Herget (2005), (4) Reuther et al. (2006), (5) Xu et al. (2009), (6) Xu (2010), and (7) Zhao et al. (2013). Red boxes with numbers denote the locations of Figures 3–6. The background topographic data consist of the Aster Global Digital Elevation Model (AGDEM). Contemporary glacier extent is from the Randolph Glacier Index (RGI) (Arendt et al., 2012).

Several reviews have summarized the results of previous studies of the extent of Pleistocene glaciations in the Altai (e.g. Butvilovkuy, 1993; Lehmkuhl et al., 2004; Lehmkuhl, Klinge, & Stauch, 2011; Lehmkuhl & Owen, 2005; Owen, 2013; Rudoy & Rusanov, 2012). Estimates of ice extent during the global last glacial maximum, based on interpretations of geomorphological and sedimentological evidence, range from a hypothesized large ice sheet terminating below the northwestern foothills close to Gorno Altaysk (Fig. 8 in Grosswald, Kuhle, & Fastook, 1994; Fig. 2 in Grosswald & Rudoy, 1996; Rudoy, 2002), to limited alpine glaciation with the largest extent in the western Russian Altai (e.g. Baryshnikov, 1992; Butvilovkuy, 1993; Lehmkuhl & Owen, 2005; Lehmkuhl et al., 2004). In central parts of the Russian Altai, the main rivers were dammed by advances of valley glaciers into the Kurai and Chuya basins, impounding large glacial lakes (e.g. Herget, 2005; Rudoy, 2002).

Determinations of the timing of past changes in glacier extent in the Altai have relied primarily on radiocarbon dating, with a few recent studies using cosmogenic nuclide, optically

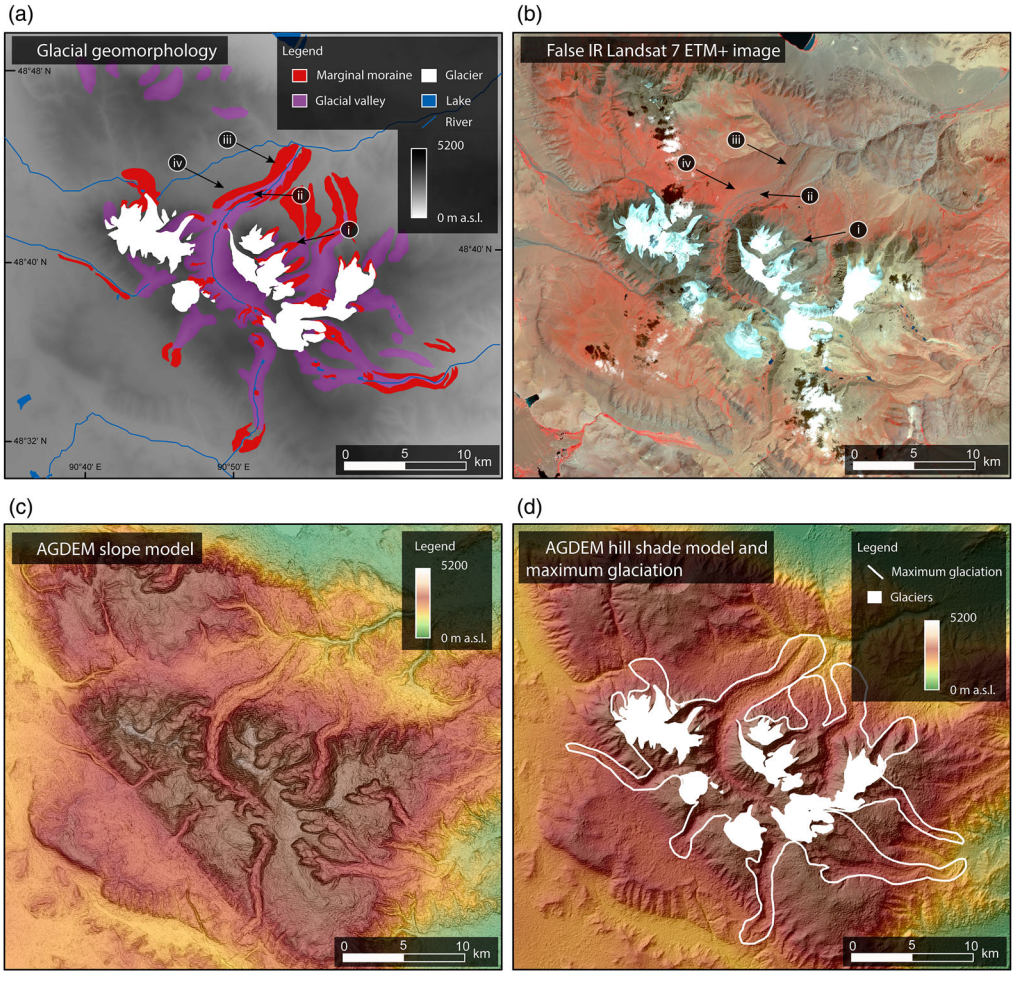

Figure 3. The Tsambagarav Massif (See Fig. 2 for location). (a) Mapped landforms and a gray-scale AGDEM (b) False IR Landsat 7 ETM+ image, (c) coloured AGDEM draped by a semi-transparent gray-scale slope model, and (d) coloured AGDEM draped by a semi-transparent gray-scale hillshade model and with the maximum paleo-glacier reconstruction from the landform record (panel a) superimposed. Roman numbers indicate examples of (i) freshly exposed latero-frontal moraine and medial supra glacial moraine, (ii) marginal moraine, (iii) large degraded marginal moraine, and (iv) large lateral moraine.

stimulated luminescence (OSL), and electron spin resonance dating (e.g. Reuther et al., 2006; Rusanov & Orlova, 2013; Zhao et al., 2013). Reuther et al. (2006) provide some of the few existing cosmogenic nuclide dates from the Russian Altai in an attempt to constrain the timing of glacial lake drainage events using cosmogenic *in situ* ^{10}Be dating of glacial lake drop stones. They conclude that the most recent flooding event has occurred at around 15 ka as a result of general warming and ice dam break-up. In the Altai region, numerous radiocarbon ages for wood, charcoal, and detritus constrain the ages of Holocene glacial deposits. Agatova et al. (2014) give an account of Holocene glacier dynamics in the southeastern Russian Altai, determined from radiocarbon dating, lichenometry, and dendrochronology while Rusanov and Orlova (2013) provide an inventory of radiocarbon ages from the Altai.

Lehmkuhl, Frechen, and Zander (2007) provide evidence for two Pleistocene glacial advances of similar extent in the Russian and Mongolian Altai, during Marine Oxygen Isotope Stage (MIS)

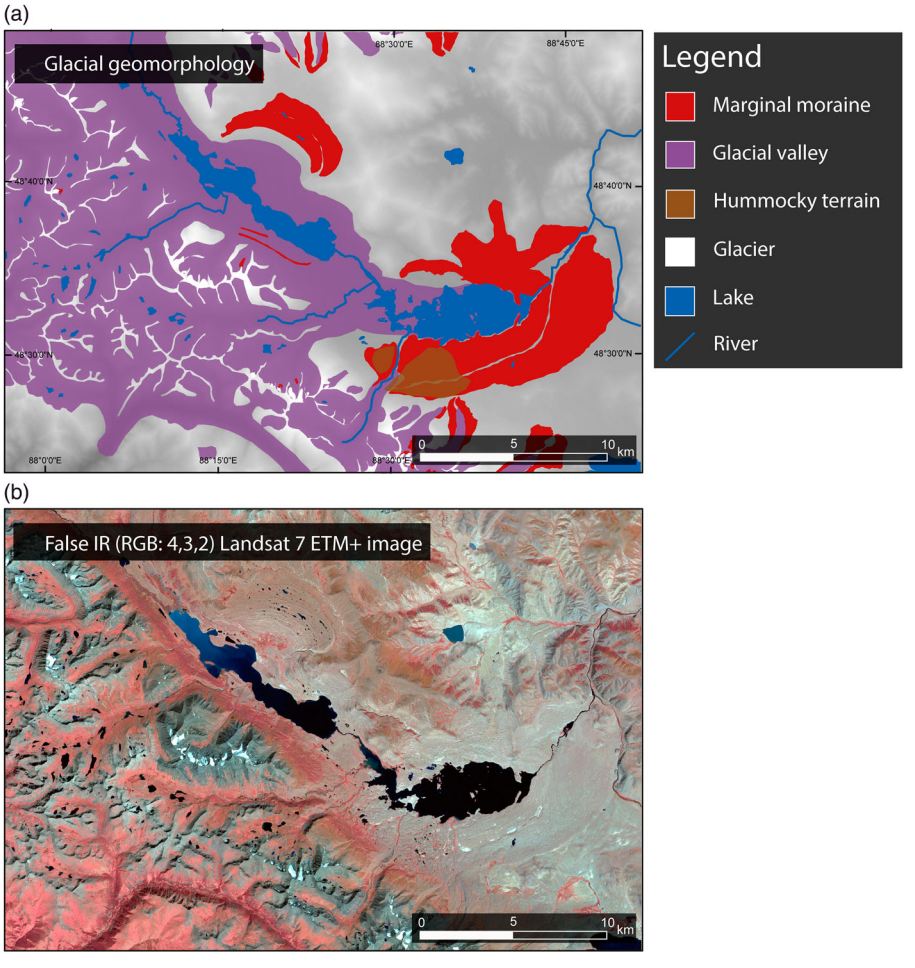

Figure 4. The Tavan Bogd marginal moraine complex (see Fig. 2 for location). (a) Mapped landforms. (b) False IR Landsat 7 ETM+ image.

2 (11–24 ka) and MIS 4 (60–71 ka). In the Chinese Altai, two recent studies yield constraints on several former glaciations in the Kanas Lake area (Xu, Yang, Dong, Wang, & Miller, 2009; Zhao et al., 2013). Combining OSL dating of sand in moraine deposits and geomorphological mapping, Xu et al. (2009) differentiate between three glacial stages recorded as a sequence of marginal moraines at the outlet of Lake Kanas. Their results indicate preservation of a late MIS 2 event and two MIS 3 (24–60 ka) events. Zhao et al. (2013) also used OSL dating of glacial deposits in the Kanas River valley and found evidence of extensive glacial advances during MIS 3 and MIS 4, arguing that the local last glacial maximum occurred during MIS 4. Zhao et al. (2013) also report electron spin resonance dating ages from Xu (2010) for a moraine complex in a tributary valley dating to MIS 6 (130–180 ka). Thus, the existing work suggests important spatial variations in the timing and number of events recorded by glacial landforms across the Altai; however, far more work is required to elucidate these patterns. Such work is most effectively pursued when study sites can be selected on the basis of systematic mapping of the landforms.

Devyatkin (1965) compiled the first map of past glaciation in the Altai, and this showed a restricted extent for Quaternary glaciations in the Russian Altai. Later, Okishev (1982, 2011)

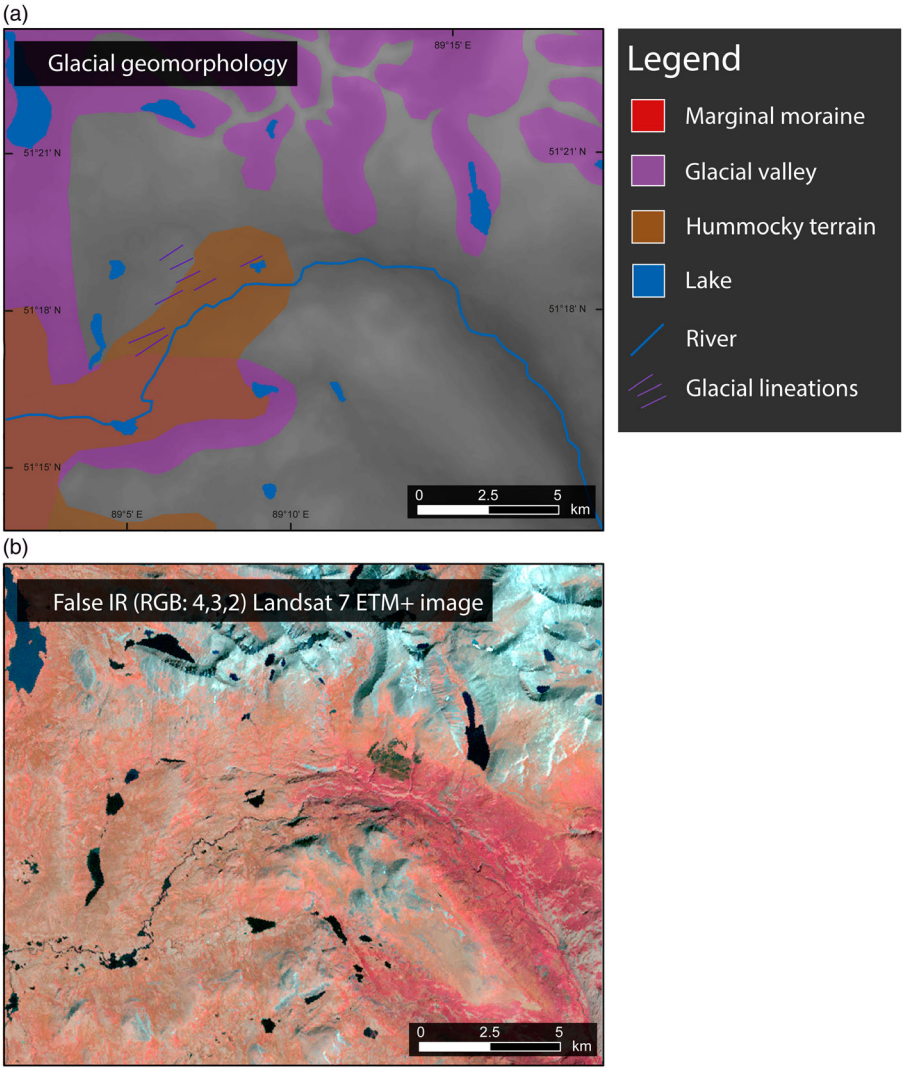

Figure 5. Glacial lineations in the northern Russian Altai (see Fig. 2 for location). (a) Mapped landforms. (b) False IR Landsat 7 ETM+ image.

published a sketch map of a more extensive glaciation, estimating the total glacier coverage for the Russian Altai as 35,000 km^2. This map was based on geomorphological evidence for ice extent during the last glacial maximum and covers a similar area to that of our study. A more recent map of Quaternary glaciation in the Russian Altai, including the Sayan Mountains and parts of the Chinese and Mongolian Altai, was produced at a scale of 1:5,000,000 in the World Atlas of Snow and Ice Resources (1997) and indicates extensive ice sheet style glaciation (cf. Fig. 8 in Grosswald et al., 1994; Fig. 2 in Grosswald & Rudoy, 1996; Rudoy, 2002).

The purpose of our work is to develop a detailed map of glacial erosional and depositional landforms that are keys to paleoglaciological studies and to provide a framework to develop detailed glacial reconstructions of the Altai Mountains. While earlier published maps focused mainly on country-specific parts of the Altai, here we present a cross-border glacial

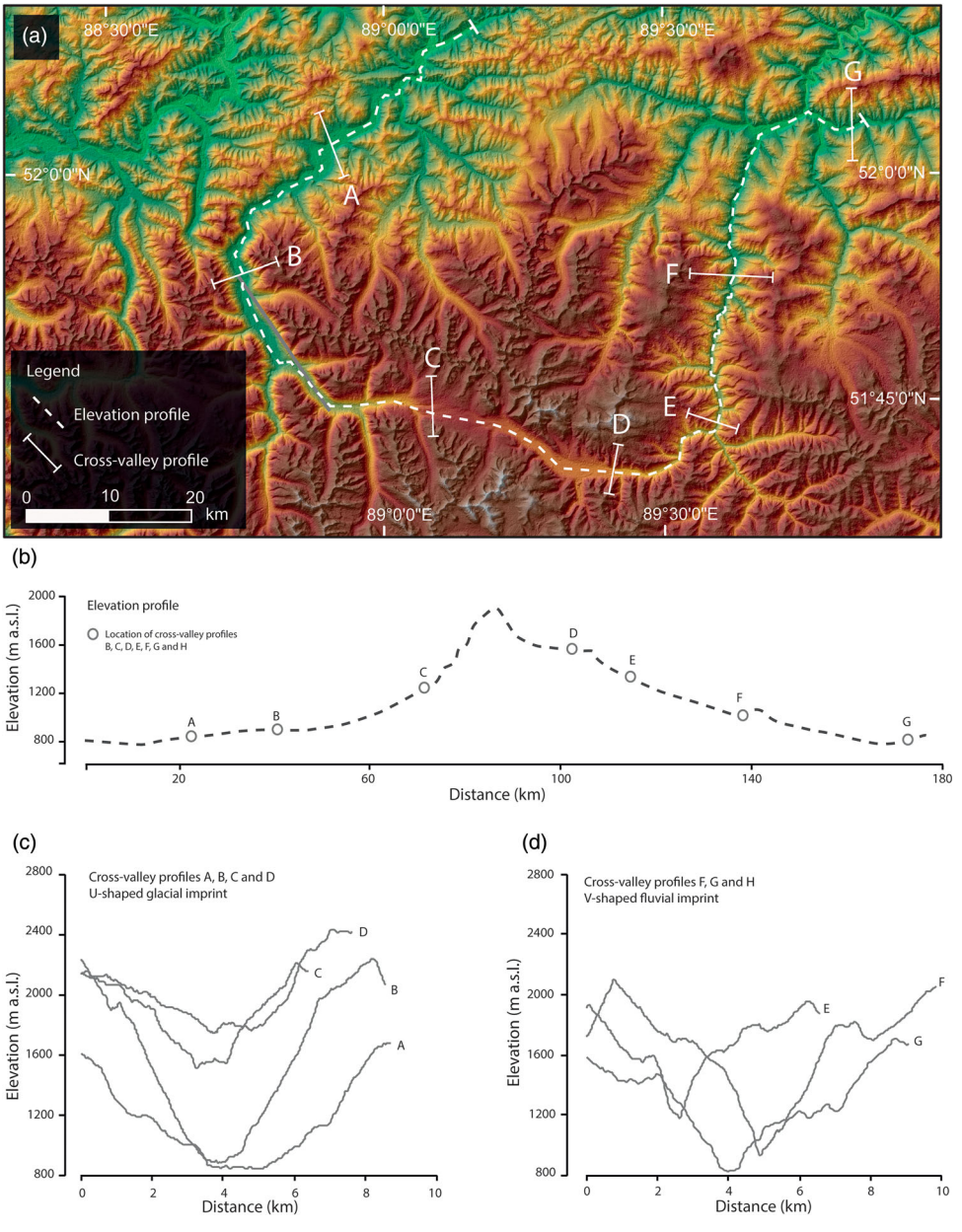

Figure 6. Interaction between glacial and fluvial processes in the Western Sayan Mountains (see Fig. 2 for location). Colured AGDEM draped by a semi-transparent gray-scale slope model with a dashed white line showing the longitudinal elevation profile (b) and non-dashed lines showing location of cross-valley profiles in (c) and (d). Profiles A, B, C, and D show a smoother U-shaped glacial imprint while profiles E, F, G, and H show a clear V-shaped fluvial imprint in their cross-valley section.

geomorphological map covering an area of 600,000 km^2, including the Russian, Chinese, and Mongolian Altai as well as the Western Sayan Mountains (Figures 1and 2). Such a map is invaluable for efforts to locate target sites of strategic importance for paleoglaciological reconstruction, to build robust glacial chronologies, and subsequently to infer paleoclimate. We also provide

preliminary estimates of the footprint of the maximum extent of glaciation based on the distribution of the glacial landforms. This map is part of a series being produced for Central Asia and Tibet using a consistent methodology (Figure 1; including Fu, Heyman, Hättestrand, Stroeven, & Harbor, 2012; Heyman, Hättestrand, & Stroeven, 2008; Morén, Heyman, & Stroeven, 2011; Stroeven, Hättestrand, Heyman, Kleman, & Morén, 2013).

2. Methods

2.1. *Mapping and data processing*

The glacial geomorphology of the Altai was mapped using visual interpretation of remotely sensed data following a pre-defined set of criteria (see section 2.2 and Heyman et al., 2008). A combination of Landsat 7 ETM+ imagery (30 m resolution) and the ASTER Global DEM (AGDEM, 30 m resolution) was used as the primary data source. All mapping was performed and compiled using on-screen digitizing of landforms. For satellite images with a high percentage of cloud cover and in areas with complex landform assemblages, additional mapping was accomplished using Google Earth's perspective viewing capability.

The mapping was performed at on-screen scales ranging from 1:30,000 to 1:60,000. Multiple RGB band combinations were used in the mapping, including both 'true' (RGB: 5,4,2) and 'false' Infra Red (IR) (RGB: 4,3,2) colour composites of Landsat 7 ETM+ imagery. False IR colour composites were found to work best because this combination yields the largest contrast between ice/snow, bedrock, and vegetation (cf. Glasser & Jansson, 2005). Furthermore, standard image enhancement procedures for satellite imagery, such as contrast stretching and histogram equalization, were adopted to improve the landform spectral signature strength (Jansson & Glasser, 2005). Finally, we also performed pan sharpening of the false IR colour composites using the panchromatic band (15 m resolution) to significantly enhance the sharpness of the imagery. A semi-transparent layer of satellite imagery was draped over the AGDEM data in an ESRI ArcGIS 10.1 environment to aid landform interpretation in complex topography (Glasser & Jansson, 2008). From the AGDEM data, we computed hillshade models to simulate solar shading and slope models to display slope steepness. To best enhance the topographic signature, these models were set to grey-scale colour ramps, with 50% transparency and draped over the original AGDEM data. All data used to aid the ;mapping are listed in the Main Map. The mapping was checked in several key areas during 2013 field investigations in the Russian, Chinese, and Mongolian Altai (Figure 2).

2.2. *Landform identification*

Four landform categories were mapped: marginal moraines, hummocky terrain, glacial lineations, and glacial valleys. Our landform descriptions are largely based on the landform descriptions of previous Tibetan Plateau and Central Asia maps (Fu et al., 2012; Heyman et al., 2008; Morén et al., 2011; Stroeven et al., 2013). However, in addition to providing definitions of each landform class, we also provide their paleoglaciological significance, descriptions of their spectral signature (morphology and colour/structure/texture) and identify possible identification errors.

Marginal moraines are landforms formed by the deposition or deformation of glacigenic sediment accumulations at the margins of active glacier snouts (Benn & Evans, 2010). Correct identification of moraines allows reconstructions of former glacier margin geometries. For the purpose of this regional study, no attempt has been made to separate between different sub-types of moraines (cf. Benn & Evans, 2010). Hence, this landform class includes a broad range of moraine types, from freshly exposed moraines (marginal and medial supra glacial moraines with no

vegetation cover (Figure 3(a) and 3(b) [i]), to latero-frontal cross-valley ridges (Figure 3(a) and (b) [ii]) and large degraded moraine complexes (Figure 3(a) and 3(b) [iii])). The morphology of these features varies dramatically from single to multiple ridges, asymmetric in cross-section, and linear, curved, sinuous, or saw-toothed in plan form, to larger sediment complexes where valleys widen (sometimes piedmont-style complexes; e.g. Barr & Clark, 2012). Moraine sizes vary from smaller ridges with areas less than 1 m^2 wide and 10 m^2 long to larger complexes of more than 100 km^2. Moraines are mainly identified in Landsat imagery and the AGDEM hill-shade model (Figure 3(b) and 3(c)). Identification criteria include shadowing due to changes in topography (relative relief) and changes in colour due to changes in soil, soil moisture, and vegetation cover. Associated landforms such as deflected abandoned meltwater channels are also useful in delineating the break-of-slope of these features. Freshly exposed latero-terminal moraines and larger moraine complexes are most easily identified, while the resolution of the Landsat imagery and AGDEM limits the complete identification of small recessional and push type moraines on valley floors. Identification errors largely involve mistakes in delineating the proper spatial extent of lateral moraines when till covers become too thin and fragmented on valley slopes and interfluves (Figure 3(a) and 3(b) [iv]).

Hummocky terrain refers to irregularly shaped sedimentary deposits consisting of rounded or elongated hills and depressions containing both till and water-lain sediments (Heyman et al., 2008). The paleoglaciological significance of hummocky terrain has been debated strongly in the literature and a number of processes have been proposed for its formation (Benn & Evans, 2010). For this study area, there is evidence of deposition by stagnant ice because the hummocky terrain usually appears in association with both the ice distal and proximal part of marginal moraines. Identification of hummocky terrain was mainly carried out using Landsat imagery (Figure 4). A high frequency of lakes and variations in soil moisture and vegetation cover between depressions and mounds are important identification criteria. Permafrost processes have been suggested to have a significant postglacial effect on glacial deposits, including lake and peat land formation in existing depressions (Sheinkman, 2011). Marginal moraine complexes might have been periglacially reworked as buried ice degrades (large number of lakes) and they can therefore potentially be misinterpreted as hummocky terrain.

Glacial lineations form a landform class that includes a range of elongated erosional and depositional ridges, aligned parallel to ice flow and formed by subglacial streamlining (Benn & Evans, 2010). The paleoglaciological significance of these features includes their relation to past ice flow directions, remoulding of the subglacial terrain, and thermal conditions at the glacier bed. Identification of glacial lineations has been based on Landsat imagery, Google Earth, and the AGDEM (Figure 5). Identification criteria include landform elongation, shadowing caused by the change in relative height, and changes in colour due to variations in soil, soil moisture, and vegetation cover of the ridges relative to depressions. Possible identification errors are confusion with non-glacial elongated bedrock features and tectonic structures.

Glacial valleys are large-scale erosional landforms with clear U-shaped cross-sections caused by large-scale erosion of ice in valleys (Li et al., 2005 and references therein). Cirques, with amphitheatre-shaped valley heads and glacial troughs (U-shaped valleys with larger dimensions and more gentle relief, cf. Heyman et al. 2008) are also included in this category. The flat valley floors and steep valley walls of glacial valleys are a result of glacial erosion rates being proportional to basal sliding velocities and ice thickness, causing the most rapid erosion to be localized to the valley centre and to decrease rapidly up valley slopes (Harbor, 1992; Li et al., 2005). Basal thermal temperatures of a glacier system control the efficiency of glacial erosion. For example, a cold-based glacier has very low sliding velocities or is completely frozen to the bed and therefore leaves poorly developed glacial landforms behind. Warm-based glaciers, on the other hand, leave behind well-developed glacial landscapes. Glacial valleys develop on

time scales of several glacial cycles and therefore signify areas that have been glaciated multiple times in the past (Li et al., 2005). Identification of glacial valleys has primarily been based on the AGDEM slope model and Google Earth (Figure 3). The appearance of the steep slopes of glacial valleys in the AGDEM slope model differs distinctly from non-glacial valleys formed by tectonic action and/or fluvial incision (Figure 6). However, the main uncertainty in delineating glacial valleys occurs for intermediate cases, when glacial valleys have tectonic origins or where glacial valleys retain fluvial imprints. A second uncertainty in glacial valley identification resides in delineating the lowest extent (downvalley) of clear glacial erosion, in other words, the transitional region where postglacial fluvial incision has started to affect the valley-cross profile but where the glacial signature is still retained. Therefore, when the signature of glacial erosion is poorly reflected in the slope- and elevation data sets this could reflect that fluvial incision and non-glacial hill slope processes have been effective, destroying the original U-shaped profile (Stroeven et al., 2009). In key valleys, the ArcGIS topographic profile tool was used to analyse the transition from glacial to fluvial/tectonic control on valley cross-section (Figure 6).

2.3. *Consistency and accuracy of mapping*

One inevitable factor affecting the consistency and accuracy of glacial geomorphological mapping is the skill and experience of the observer (Smith & Wise, 2007). In order to minimize this bias, Blomdin performed all of the mapping with key areas being mapped by the co-authors as well, thus increasing consistency and accuracy, and ensuring comparability with the previous mapping efforts (Fu et al., 2012; Heyman et al., 2008; Morén et al., 2011; Stroeven et al., 2013). The mapping has been performed with multiple passes over the study area using different data sets and a range of scales to increase consistency. Another factor affecting mapping accuracy is the resolution of the data sets. The resolution of the Landsat 7 ETM+ imagery is about 30 m for the colour bands and 15 m for the panchromatic band (number 8). The resolution of the AGDEM is also 30 m; hence, landforms smaller than 30 m have not been mapped.

2.4. *Delineation of past ice margins*

As a first step to reconstruct past glacier dimensions in the Altai Mountains, we have estimated the aerial extent of glaciation based on the distribution of glacial landforms. A manual delineation was performed within a geographical information system (GIS) using the margins of glacial valleys, moraines, and other glacial features as a guide for maximum glacier extent (Figure 3(d); Figure 7). This method enables a straightforward delineation of maximum glacier extent in formerly glaciated mountain regions using mapped glacial landforms. Our reconstruction is strictly remote sensing based and represents the minimum extent of maximum glaciation (cf. Heyman et al., 2009). We are aware that glacial deposits may extend well beyond our reconstructed paleo-glacier limits, which reinforces our inference that the mapped extent of maximum glaciation is its minimum footprint. When working with extensive regions like the Altai Mountains, this paleoglaciological footprint yields a useful estimate of past glacier coverage based on the distribution of landforms and allows for a comparison with present-day glacier extent (e.g. Bussemer, 2000; Klinge, 2001; Okishev, 2006; Shi, 1992). In this study, we compare our reconstructed paleo-glacier extents with contemporary glacier areas calculated from the Randolph Glacier Inventory (RGI) V 3.2 (Arendt et al., 2012). When reconstructing former glacier extents in individual mountain massifs or in formerly glaciated catchments, there is a need for detailed reconstructions that consider the effects of topography and glacier physics (e.g. Barr & Clark, 2011; Ng, Barr, & Clark, 2010).

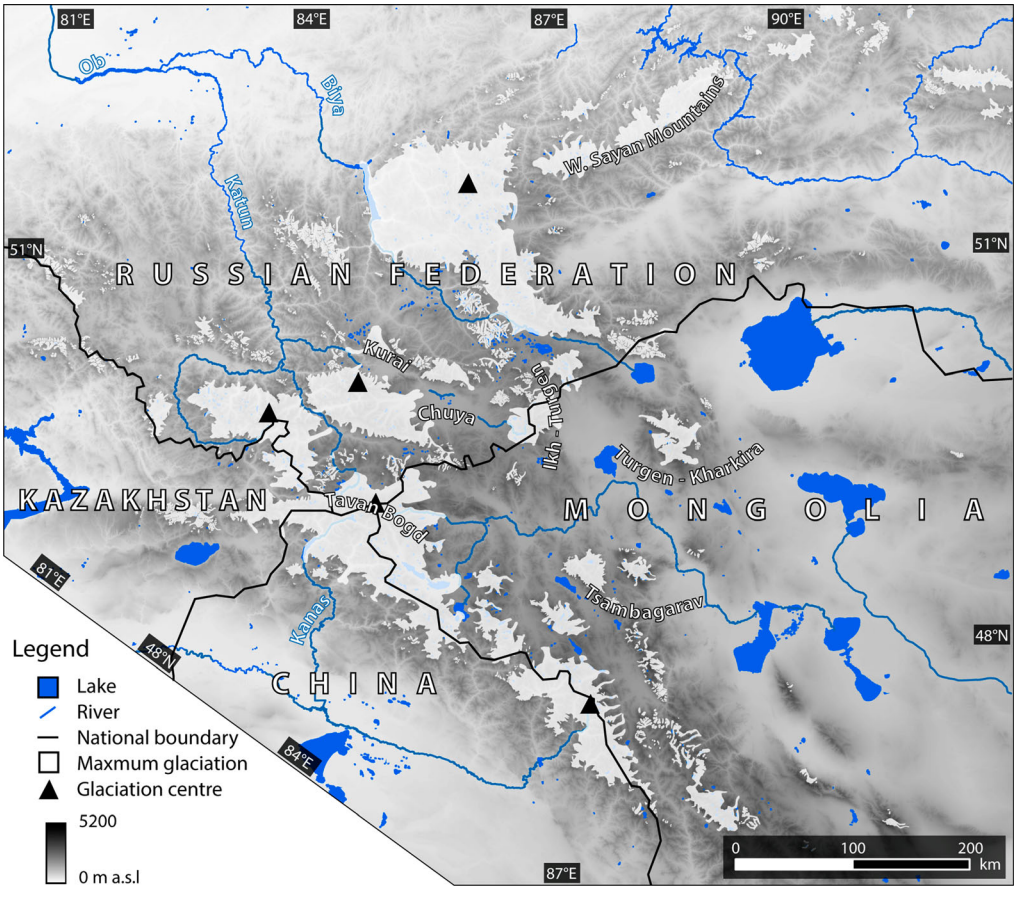

Figure 7. Minimum extent of maximum glaciation and inferred glaciation centres in the Altai and Western Sayan Mountains.

3. Discussion and conclusions

We present a glacial geomorphological map of the Altai and Western Sayan Mountains, covering an area of almost 600,000 km^2. We mapped four types of glacial landforms: marginal moraines, glacial lineations, hummocky terrain, and glacial valleys. Moraines cover a total area of about 2900 km^2, which is about 0.5% of the study area. In total, we identified 1522 individual marginal moraine polygons. Large terminal moraine complexes are mainly located in intermontane basins, outside of the main mountain massifs and were likely formed by several glacial advances. One example of a terminal moraine complex is situated in northwestern Mongolia, and originates from a glacier tongue draining the Tavan Bogd catchment, on the Chinese-Mongolian border (Figure 4). Glacial valleys, on the other hand, cover an area of about 47,000 km^2 (8.0% of the study area) while areas of hummocky terrain total 980 km^2 (less than 0.2% of the study area). Glacial lineations appear infrequently in the study area. In total, we identified only 21 glacial lineations, which may indicate that lineations in this area are absent or smaller than 30 m.

The distribution of glacial valleys and marginal moraines indicates that the Altai Mountains experienced alpine-style glaciations in the past, with centres of glaciation consisting of ice caps and ice fields centred on the higher mountain areas (Figure 7).

Based on the Randolph Glacier Inventory (Arendt et al., 2012), contemporary glacier coverage for the study area is about 1300 km^2 (0.2% of the map area). By tracing the outermost limits of glaciation, as indicated by the distribution of preserved glacial landforms, we estimate the extent of minimum–maximum glaciation totalled to 65,000 km^2 (or 10.8% of the map area). This estimate does not represent ice coverage for one particular point in time but rather the cumulative effect of glaciation during Quaternary glacial cycles. Other estimates of maximum glacier coverage range from 35,000 km^2 (Bussemer, 2000) to 80,000 km^2 (Lehmkuhl et al., 2004, 2011). Only the application of numerical dating methods, such as cosmogenic surface exposure or OSL dating, and detailed studies of sediments can potentially help us determine if glacier extents in Figure 7 occurred contemporaneously. In addition, glacier coverage may have been more extensive than shown in Figure 7. For example, detailed field investigations might reveal sediment-landform patterns that are not detected in the remote sensing-based mapping outside of our reconstructed ice margins.

The map resulting from this work demonstrates the usefulness of remote sensing techniques for mapping glacial geomorphology in rugged and poorly accessible areas, such as the Altai Mountains, and in quantifying the extent of former glaciation. The map has been used to guide the detailed field investigations that are designed to provide robust paleoglaciological reconstructions.

Software

ESRI ArcGIS 10.1 was used for data pre-processing, mapping, and on-screen landform digitization. Additional on-screen landform identification was performed using Google Earth, which allows perspective viewing of the landscape. The final layout of the map was designed in Adobe Illustrator CS6 following the same cartographic layout as Heyman et al. (2008), Morén et al. (2011), Fu et al. (2012) and Stroeven et al. (2013).

Data

The authors have supplied data (as ESRI Shapefiles) used in the production of the accompanying map.

Funding

This work was supported by a Swedish Research Council grant (No. 2011-4892) to Arjen P Stroeven. Additional funding for fieldwork in 2013 and 2014 was supported by stipends from The Swedish Society for Anthropology and Geography (SSAG), Carl Mannerfelts Fund, Margit Alhtin Scholarship Fund, and Geerard De Geers Fund to Robin Blomdin and Natacha Gribenski.

References

Agatova, A. R., Nepop, R. K., Slyusarenko, I. Y., Myglan, V. S., Nazarov, A. N., & Barinov, V. V. (2014). Glacier dynamics, palaeohydrological changes and seismicity in southeastern Altai (Russia) and their influence on human occupation during the last 3000 years. *Quaternary International*, *324*, 6–19. doi:10.1016/j.quaint.2013.07.018

Arendt, A., Bolch, T., Cogley, J. G., Gardner, A., Hagen, J.-O., Hock, R., … Zheltyhina, N. (2012). *Randolph Glacier Inventory – a dataset of global glacier outlines: Version 3.2. Global Land Ice Measurements from Space*. Boulder, CO: Digital Media.

Barr, I. D., & Clark, C. D. (2011). Glaciers and climate in Pacific Far NE Russia during the Last Glacial Maximum. *Journal of Quaternary Science*, *26*(2), 227–237. doi:10.1002/jqs.1450

Barr, I. D., & Clark, C. D. (2012). Late quaternary glaciations in Far NE Russia; combining moraines, topography and chronology to assess regional and global glaciation synchrony. *Quaternary Science Reviews*, *53*, 72–87. doi:10.1016/j.quascirev.2012.08.004

Baryshnikov, G. J. (1992). *Die Entwicklung des Reliefs der Übergangszonen von Bergländern im Kanäozoikum* (p. 181). Tomsk: University of Tomsk Press (in German).
Benn, D. I., & Evans, D. J. A. (2010). *Glaciers and glaciation* (2nd ed., p. 802). London: Routledge.
Bussemer, S. (2000). Jungquartäre Vergletscherung im Bergaltai und inangrenzenden Gebirgen – analyse des Forschungsstandes. *Mitteilungen der Geographischen Gesellschaft in München*, *85*, 45–64 (In German).
Butvilovkuy, V. V. (1993). *Paleogeography of Last Glaciation and Holocene of Altai: event-catastrophic model* (p. 253). Tomsk: Tomsk University Press (In Russian).
Devyatkin, Y. V. (1965). *Cenozoic sediments and neotectonics of South-Eastern Altai* (p. 243). Moscow: Nauka (In Russian).
Dolgushin, L. D., & Osipova, G. B. (1989). *Glaciers* (p. 447). Moscow: Mir (In Russian).
Fu, P., Heyman, J., Hättestrand, C., Stroeven, A. P., & Harbor, J. M. (2012). Glacial geomorphology of the Shaluli Shan area, southeastern Tibetan Plateau. *Journal of Maps*, *8*(1), 48–55.
Glasser, N. F., & Jansson, K. N. (2005). Fast-flowing outlet glaciers of the last glacial maximum patagonian icefield. *Quaternary Research*, *63*(2), 206–211. doi:10.1016/j.yqres.2004.11.002
Glasser, N. F., & Jansson, K. (2008). The glacial map of southern South America. *Journal of Maps*, *4*(1), 175–196. doi:10.4113/jom.2008.1020
Grosswald, M. G., Kuhle, M., & Fastook, J. L. (1994). Würm glaciation of Lake Issyk-Kul Area, Tian Shan Mts.: a case study in glacial history of central Asia. *GeoJournal*, *33*, 273–310.
Grosswald, M. G., & Rudoy, A. N. (1996). Quaternary glacier-dammed lakes in the mountains of Siberia. *Polar Geography*, *20*(3), 180–198. doi:10.1080/10889379609377599
Harbor, J. M. (1992). Numerical modeling of the development of U-shaped valleys by glacial erosion. *Geological Society of America Bulletin*, *104*, 1364–1375. doi:10.1130/0016-7606(1992)104<1364
Herget, J. (2005). *Reconstruction of Pleistocene Ice-Dammed Lake outburst floods in the Altai Mountains, Siberia*, GSA Special Paper 386, 118 p. Boulder, CO: GSA Inc.
Heyman, J., Hättestrand, C., & Stroeven, A. P. (2008). Glacial geomorphology of the Bayan Har sector of the NE Tibetan Plateau. *Journal of Maps*, *4*, 42–62.
Heyman, J., Stroeven, A. P., Alexanderson, H., Hättestrand, C., Harbor, J., Li, Y., … Machiedo, M. (2009). Palaeoglaciation of Bayan Har Shan, northeastern Tibetan Plateau: glacial geology indicates maximum extents limited to ice cap and ice field scales. *Journal of Quaternary Science*, *24*, 710–727. doi:10.1002/jqs
Jansson, K. N., & Glasser, N. F. (2005). Using Landsat 7 ETM + imagery and Digital Terrain Models for mapping glacial lineaments on former ice sheet beds. *International Journal of Remote Sensing*, *26*(18), 3931–3941.
Kamp, U., McManigal, K. G., Dashtseren, A., & Walther, M. (2013). Documenting glacial changes between 1910, 1970, 1992 and 2010 in the Turgen Mountains, Mongolian Altai, using repeat photographs, topographic maps, and satellite imagery. *The Geographical Journal*, *179*(3), 248–263. doi:10.1111/j.1475-4959.2012.00486.x
Klinge, M. (2001). Glazialgeomorphologische Untersuchungen im Mongolischen Altai als Beitrag zur jungquartären Landschafts – und Klimageschichte der Westmongolei. *Aachener Geographische Arbeiten*, *35*, 125 p. Aachen: Aachen Geographiches Institut (In German).
Lehmkuhl, F., Frechen, M., & Zander, A. (2007). Luminescecne chronology of fluvial and aeolian deposits in the Russian Altai (Southern Siberia). *Quaternary Geochronology*, *2*, 195–201.
Lehmkuhl, F., Klinge, M., & Stauch, G. (2004). The extent of Late Pleistocene glaciations in the Altai and Khangai Mountains. In J. Ehlers & P. L. Gibbard (Eds.), *Quaternary Glaciations – Extent and chronology, Part III* (1st ed., pp. 243–454). Amsterdam: Elsevier B. V.
Lehmkuhl, F., Klinge, M., & Stauch, G. (2011). The extent and timing of Late Pleistocene Glaciations in the Altai and neighboring mountains systems. In J. Ehlers & P. L. Gibbards (Eds.), *Development in Quaternary science – Extent and chronology – A closer look* (Vol. 15, pp. 967–979). Amsterdam: Elsevier B. V.
Lehmkuhl, F., & Owen, L. A. (2005). Late Quaternary glaciation of Tibet and the bordering mountains: a review. *Boreas*, *34*(2), 87–100. doi:10.1080/03009480510012908
Li, Y., Harbor, J., Stroeven, A. P., Fabel, D., Kleman, J., Fink, D., … Elmore, D. (2005). Ice sheet erosion patterns in valley systems in northern Sweden investigated using cosmogenic nuclides. *Earth Surface Processes and Landforms*, *30*(8), 1039–1049. doi:10.1002/esp.1261
Morén, B., Heyman, J., & Stroeven, A. P. (2011). Glacial geomorphology of the central Tibetan Plateau. *Journal of Maps*, *7*(1), 115–125. doi:10.4113/jom.2011.1161

Ng, F. S. L., Barr, I. D., & Clark, C. D. (2010). Using the surface profiles of modern ice masses to inform palaeo-glacier reconstructions. *Quaternary Science Reviews*, *29*(23–24), 3240–3255. doi:10.1016/j.quascirev.2010.06.045

Okishev, P. A. (1982). *Dynamics of Altai Glaciation in Late Pleistocene-Holocene* (p. 209). Tomsk: Tomsk State University
(In Russian).

Okishev, P. A. (2006). Topography and glaciation Russian Altai. In P. A. Okishev & J. K. Narozhnyi (Eds.), *Problems of geography of Siberia* (pp. 39–55). Tomsk: Tomsk University Press.

Okishev, P. A. (2011). *Relief and glaciation of Russian Altai* (p. 420). Tomsk: Tomsk University Press. (In Russian).

Owen, L. A. (2013). Late Quaternary in Highland Asia. In S. A. Elias (Ed.), *Encyclopedia of quaternary science* (2nd ed., pp. 236–244). Amsterdam: Elsevier B. V. doi:10.1016/B978-0-444-53643-3.00119-9

Reuther, A. U., Herget, J., Ivy-Ochs, S., Borodavko, P., Kubik, P. W., & Heine, K. (2006). Constraining the timing of the most recent cataclysmic flood event from ice-dammed lakes in the Russian Altai Mountains, Siberia, using cosmogenic in situ ^{10}Be. *Geology*, *34*(11), 913–916. doi:10.1130/G22755A.1

Rudoy, A. N. (2002). Glacier-dammed lakes and geological work of glacial superfloods in the Late Pleistocene, Southern Siberia, Altai Mountains. *Quaternary International*, *87*, 119–140.

Rudoy, A. N., & Rusanov, G. G. (2012). *Last glaciations of North-West Altai. Koksa River catchment* (p. 240). Tomsk: NTL.

Rusanov, G. G., & Orlova, L.A. (2013) *Radiocarbon dates (SOAN) Gorny Altai and Altai Foreplain* (p. 291). Bijsk: AGAO Publisher. (In Russian).

Sheinkman, V. S. (2011). Glaciation in the high mountains of Siberia. In S. A. Elias (Eds.), *Quaternary glaciations – extent and chronology* (1st ed., pp. 883–907). Amsterdam: Elsevier, B. V.

Shi, Y. (1992). Glaciers and glacial geomorphology in China. *Zeitschrift für Geomorphologie N.F Supplement Band*, *86*, 51–63.

Smith, M. J., & Wise, S. M. (2007). Problems of bias in mapping linear landforms from satellite imagery. *International Journal of Applied Earth Observation and Geoinformation*, *9*, 65–78.

Stroeven, A. P., Hättestrand, C., Heyman, J., Harbor, J., Li, Y. K., Zhou, L. P., … Liu, G. N. (2009). Landscape analysis of the Huang He headwaters, NE Tibetan Plateau – patterns of glacial and fluvial erosion. *Geomorphology*, *103*(2), 212–226. doi:10.1016/j.geomorph.2008.04.024

Stroeven, A. P., Hättestrand, C., Heyman, J., Kleman, J., & Morén, B. M. (2013). Glacial geomorphology of the Tian Shan. *Journal of Maps*, *9*(4), 505–512. doi:10.1080/17445647.2013.820879

Tronov, M. V. (1949). *Essays about Altai Glaciation* (p. 376). Moscow: Geographgiz. (In Russian).

Tronov, M. V. (1966). *Glaciers and climate* (p. 407). Leningrad: Gidrometeoizdat. (In Russian).

World Atlas of Snow and Ice Resources. (1997). (p. 392). Moscow: Russian Academy of Sciences (In Russian).

Xu, X., Yang, J., Dong, G., Wang, L., & Miller, L. (2009). OSL dating of glacier extent during the Last Glacial and the Kanas Lake basin formation in Kanas River valley, Altai Mountains, China. *Geomorphology*, *112*(3–4), 306–317. doi:10.1016/j.geomorph.2009.06.016

Xu, X. K. (2010). *Late Pleistocene glacial geomorphology and dating in Kanas River valley, Altai Mountains* (Unpublished Ph.D thesis). Graduate University of Chinese Academy of Sciences, Beijing (in Chinese with English abstract).

Zhao, J., Yin, X., Harbor, J. M., Lai, Z., Liu, S., & Li, Z. (2013). Quaternary glacial chronology of the Kanas River valley, Altai Mountains, China. *Quaternary International*, *311*, 44–53. doi:10.1016/j.quaint.2013.07.047